

Lipid Bilayers on Silicon Substrates

Subjects: Materials Science, Biomaterials | Materials Science, Coatings & Films | Physics, Condensed Matter

Contributor: Ulrich G. Volkmann, Marcelo Cisternas, Nancy Gómez-Vierling, Tomas Corrales

Artificial membranes are models for biological systems that are important for several applications. In the present entry we talk about artificial membranes such as supported lipid bilayers (SLB) and ways to self-assemble them. We mainly focus on the results of a new dry evaporation process in high vacuum, i.e., physical vapor deposition, to make samples of dipalmitoylphosphatidylcholine (DPPC) on silicon substrates. We have characterized the main phase transitions and adhesion of our SLBs using high-resolution ellipsometry and AFM techniques. The finding of this new SLB fabrication approach is relevant for the understanding the interaction of lipid bilayers in contact with surfaces in dry environments, with the aim to develop new kinds of lab-on-chip bionanosensors. This discovery is especially relevant in the context of the viability of organisms covered with lipid bilayer structures. An example of this kind of interaction occurs between bilayer-protected viruses, e.g., corona viruses, and solid surfaces, allowing the virus to stay active during long periods of time. The prolonged stability of SLBs on dry SiO₂/Si substrates detected in our research can explain the long-term stability of some viruses deposited or adsorbed on dry surfaces, including the SARS-CoV-2 virus.

Keywords: supported lipid bilayers ; bio-silica interfaces ; self-assembly ; phase transitions ; artificial membranes ; atomic force microscopy ; force spectroscopy ; high resolution ellipsometry ; physical vapor deposition ; SARS-CoV-2

1. Introduction

Biological membranes are one of the essential components of the cell and, consequently, all living beings. Biological- or plasma- membranes are formed from a series of lipids that act as a selective barrier in cells, bacteria, and many viruses. These lipids self-assemble into bilayer structures, forming phospholipid membranes. In addition of phospholipids, biological membranes are formed by a mixture of other lipids, such as glycolipids and cholesterol. Conventionally, biological membranes are studied under hydrated conditions, but there is also a growing interest in studying their formation and stability in air. In particular, recent attention has focused on understanding the long-term viability of viruses adsorbed on solid surfaces ^[1]. To study biological membranes and their interaction with solid surfaces in dry conditions, model systems can be created to mimic their properties, i.e., artificial membranes, that have the potential to be used for applications in the field of bionanotechnology ^[2]. This field combines nanoscale technologies with biological systems in order to create functional devices with diverse applications, such as drug delivery, biosensors, carriers of small molecules and templates for pharmaceutical design ^{[3][4][5][6][7][8][9]}. An important goal for bionanotechnology is to create silicon-based chips that can biomimic biological membranes, i.e., bio-silica interfaces ^[10]. Such a bio-silica interface could be used to study the insertion of proteins within membranes.

A first step for mimicking a plasma membrane over a solid surface is to form phospholipid bilayers, which are referred to as a supported lipid bilayer (SLB) ^[11]. One method to form a SLB is by using small vesicles, which are suspended in water or buffer solution and set to interact with a silicon surface. Once the vesicles interact with the hydrophilic silicon surface, they self-assemble into a SLB ^[12]. There have been many studies reporting different methods to form SLBs from vesicles, such as polymer cushioned lipid bilayers ^{[13][14][15][16]}, hybrid bilayers supported over alkane-thiol self-assembled monolayers (SAM) ^{[17][18]}, tethered lipid bilayers ^{[19][20]} and freely-suspended bilayers ^{[21][22]}. Another method to form SLBs, without starting from a vesicle, is using the Langmuir–Blodgett method ^[23], where a solid substrate is successively immersed within a compressed layer of lipids, which assemble at a liquid-air interface. Furthermore, a recent solvent-assisted method using isopropanol has been reported to form SLBs, where lipid molecules are dissolved in isopropanol and flowed through a liquid reaction chamber, generating a bilayer over a glass slide ^[24]. All the aforementioned methods involve the use of solvents to dissolve lipid molecules, transport small vesicles or assemble a transfer monolayer over liquid-air interfaces. The main disadvantage of liquid-based methods is that they are dependent on specific phospholipid and solvent types, concentration and surface tension between the liquid-solid interface.

Results towards the creation of a solvent-free bio-silica interface was first reported by Retamal et al. (2014) ^[25], who showed that supported bilayers of dipalmitoylphosphatidylcholine (DPPC) can be evaporated from their vapor phase over a cushion of chitosan (CH), previously evaporated onto the substrate ^[25]. Using Raman spectroscopy, Retamal et al.

showed that the evaporation process did not alter the chemical composition of the DPPC molecules [25]. Furthermore, ellipsometric measurements on these DPPC/CH/SiO₂/Si samples in air, previously hydrated with a drop of water, showed evidence of gel to ripple, ripple to liquid crystalline and liquid crystalline to fluid disordered phase transitions at 301 K, 315 K and 328 K, respectively. The reported phase transitions are consistent with previous reports in liquid [26][27][28][29][30]. Although promising, some drawbacks of the CH cushion arise due to its dynamics during evaporation. In particular, Retamal et al. showed, in a separate work, that vapor deposited CH exhibits a solid-state dewetting processes on silicon surfaces that occurs during the evaporation at room temperature [31]. Recently, Cisternas et al., reported the vapor deposition of phospholipids on a different biocompatible substrate, titanium (Ti) [32]. After a plasma immersion ion implantation and deposition treatment (PIII&D) a tiny layer of titanium nitride (TiN) was formed and a thin layer of CH was previously vapor-deposited in order to provide a moisturizing matrix for the artificial membrane of DPPC. The CH and, subsequently, the DPPC were vapor-deposited on the plasma-treated TiN substrate. The formation of artificial membranes was confirmed by atomic force microscopy (AFM), measuring the topography at different temperatures and performing force curves [32]. This previous work confirms that the nitrogen PIII&D-treated Ti can be used to support, with enhanced biocompatibility, stable phospholipid artificial membranes (SLBs) that are vapor-deposited in high vacuum.

In the present work we go one step further and omit the CH moisturizing matrix or cushion. In other words, we focus on evaporating DPPC molecules directly onto a monocrystalline silicon substrate, covered with its native SiO₂ layer, without further hydration. Our work shows that it is possible to form stable SLBs, which self-assembled without the need of further hydration and which are stable in dry conditions over weeks and at least up to nine months. The evaporation of molecules is performed in high vacuum conditions with in situ ellipsometric thickness monitoring. After the evaporation process, the chamber is vented with air and heating ramps at a rate of 2 K/min are performed. Using ellipsometry, we monitor the optical thickness of the samples and observe the characteristic phase transitions of DPPC. In parallel, AFM is used to study the morphological changes of the sample after each heating ramp. Combined AFM and ellipsometric measurements show evidence of the formation of a phospholipid bilayer system that self-assembled in dry conditions. Using AFM, we have performed force curves that show the rupture of several bilayers at increasing loads. Finally, we have observed the restructuring of the bilayer by increasing the AFM force setpoint in imaging mode. The morphology, force-dependent restructuring and rupture forces corroborate the ellipsometric measurements and point to a stable DPPC bilayer in air.

The dry, solvent free formation of SLBs without hydration in combination with an extreme long-term stability is relevant for technical applications in the field of functional biointerfaces and lab-on-chip technology, e.g., for fabrication of biosensors and membrane-protein platforms and to gain insight into the lifetime and stability of viruses protected by phospholipid bilayers, adsorbed on static solid surfaces or via airborne transmissions of inhalable particulate material (PM), tiny droplets or aerosols which contributes to the spread of COVID-19 illness virus (SARS-CoV-2).

| 2. Results

In Figure 1 we show an AFM image of DPPC as deposited over silicon and force spectroscopy curves obtained on the different evaporated regions using quantitative imaging (QITM) mode. Figure 1a shows the island-like topography of the sample right after the evaporation process. Figure 1b shows a height distribution of the topography, from where we can identify three clearly separated height levels. From these height distributions we obtain the three main peaks centred at 4.01 ± 0.93 nm (level 1), 8.08 ± 0.94 nm (level 2) and 12.17 ± 0.98 nm (level 3). These step heights are multiples of 4 nm, which is the characteristic height of a DPPC bilayers [26][33]. Figure 1c shows an adhesion map of the same region, while Figure 1d shows an adhesion distribution. From Figure 1d, we can say that the entire surface is covered with a layer that has roughly the same adhesion, i.e., only one peak is seen centred at 9 nN, this is higher than our measured value for the bare silicon substrate, on which we measure an adhesion force of 5 nN.

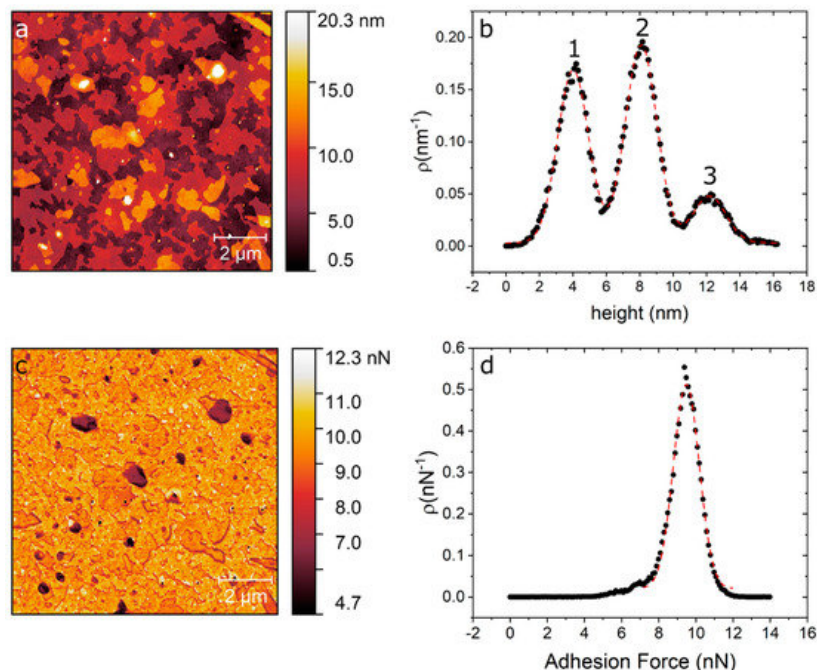


Figure 1. (a) AFM topography image of DPPC/SiO₂/Si taken directly after evaporation. (b) Height distribution of the topography map showing the three distinct levels at 4 nm, 8 nm and 12 nm. (c) Adhesion map of the same region. (d) Adhesion distribution centred at 9 nN.

In order to test the mechanical properties of the membrane in Figure 1, we performed force curves using AFM [34]. Figure 2 shows representative AFM force curves taken using force mapping mode on a 7 μm × 7 μm area. Breakthrough events are seen as sudden drops in the force curves. These breakthrough events are seen at all points, and show 1, 2 or 3 breakthrough events (Figure 2a–c), respectively. Force curves with one breakthrough are attributed to the rupture of the first level, i.e., only one bilayer (Figure 2a). Meanwhile, force curves with two and three breakthrough events are related to ruptures in levels 2 and 3 (Figure 2b,c). The rupture forces show that we have a complete coverage of the substrate with one DPPC bilayer, i.e., we always see at least one rupture event. On top of this complete bilayer we have partial coverage of two and three additional bilayers (see Figure 1a). By averaging all curves with one rupture we obtain an average of 5.3 ± 2.4 nN. Force curves showing two ruptures (level two) show a first rupture at 5.6 ± 1.2 nN followed by a second rupture at 5.1 ± 1.1 nN. Finally, force curves with three rupture events (level 3) rupture first at 5.3 ± 2.0 nN, followed by a second rupture at 5.2 ± 1.8 nN and a third rupture at 5.0 ± 1.7 nN. As seen, all ruptures in dry, non-hydrated SLBs occur around 5 nN and are independent of the number of layers. To compare the mechanical properties of SLBs immersed in liquid, we applied AFM force curves to phospholipid bilayers fabricated under the same procedure (formed by physical vapour deposition in high vacuum) immersed in pure water in the AFM JPK NanoWizard™ Heating Cooling Module HCM™ accessory. We applied tip forces up to 15 nN and no rupture of the bilayer membrane was observed.

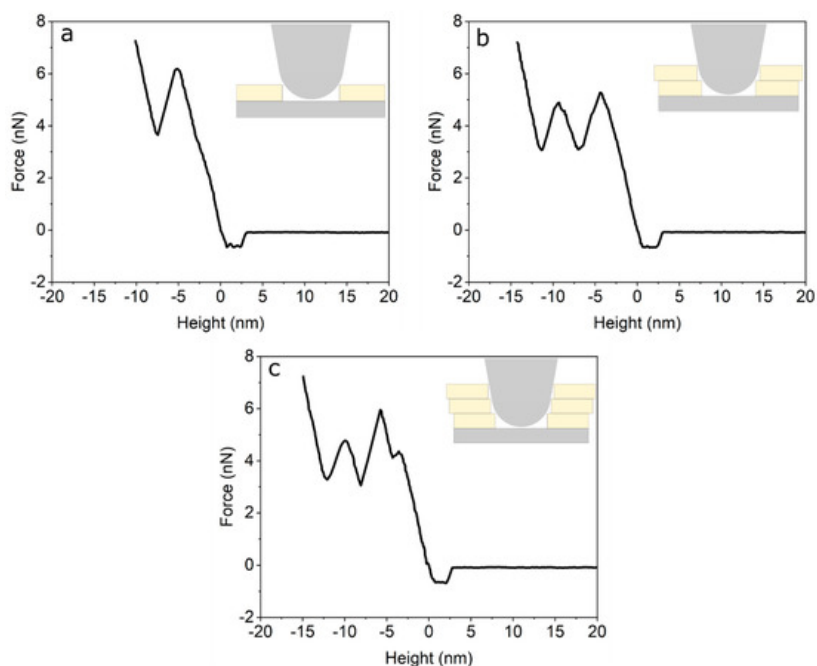


Figure 2. (a) Force curve on the first bilayer (level 1). (b) Force curve on the second bilayer (level 2). (c) Force curve on the third bilayer (level 3).

To confirm the DPPC bilayer formation, complementary ellipsometric measurements were performed in order to observe phase transitions, by applying heating and cooling temperature ramps between room temperature (RT) and 347 K. Figure 3 shows the variations in the polarizer angle (ΔP), which represents variations in the polarizability of the bilayer molecules [35]. The ellipsometric data permits, based on the models of Paul Drude [36] and the equivalent model [37] of Dignam and Fedyk [35], an interpretation of the collective behaviour on a molecular scale. Figure 3a corresponds to the first temperature ramp applied to the sample of ~ 60 Å DPPC on SiO_2/Si , while Figure 3b,c show the data obtained during the second and third heating ramp, respectively.

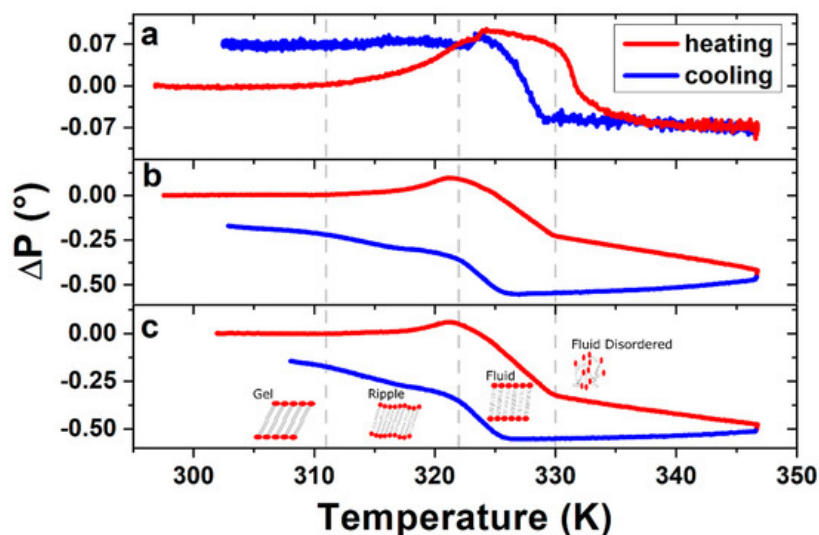


Figure 3. Ellipsometric changes in polarizer angle ΔP of DPPC bilayer, measured during (a) the first, (b) the second and (c) the third heating–cooling cycle. Vertical dashed lines indicate the phase transition temperatures as described in the text. The ΔP signal of the following heating–cooling cycles show the same characteristics of figures (b) and (c), leading to the conclusion that the structure formed after the first heating–cooling cycle remains stable.

Changes in slope, or inflection points, of the ellipsometric signal indicate changes in the phase of the DPPC bilayers. The three transitions measured in the sample corresponding to Figure 3b,c are from left to right: The gel to ripple at 311 K, ripple to liquid crystalline at 322 K and liquid crystalline to fluid disordered at 330 K, respectively, marked in Figure 3 with vertical dashed lines. Further experiments on four different samples prepared under the same conditions give us a gel to ripple transition at 311.5 ± 0.9 K, ripple to liquid crystalline at 323.8 ± 2.5 K and a liquid crystalline to fluid disordered at 330.4 ± 0.9 K.

Given that the transition seen at 311 K (gel to ripple) is a smooth continuous transition, we perform complimentary QI^{TM} AFM measurements in this low temperature range. Adhesion maps of 2×2 μm were recorded over a total of 3 SLB samples. Temperature ramps were taken using steps of 5 K, starting from room temperature to 328 K. Figure 4a–c show the adhesion maps at 296 K, 308 K and 323 K, for one of the samples. A noticeable change in adhesion is observed between images when compared in the same adhesion range (1–20 nN). By extracting the adhesion distribution at the different temperatures and obtaining the centre and half width of the distribution, we can plot the average adhesion force as a function of temperature, as shown in Figure 4d, for three representative samples. Another adhesion map used to build the graph in the Figure 4d is shown in the Figure S10. As seen in Figure 4d, the adhesion value rises between room temperature and 308–312 K and then drops abruptly.

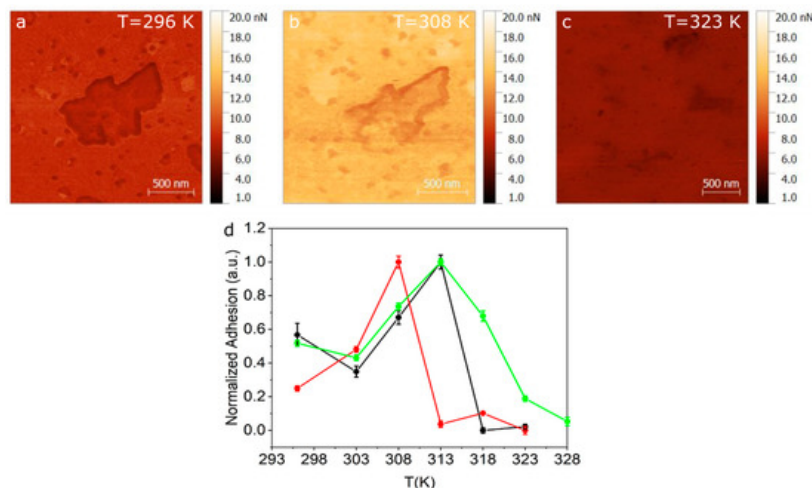


Figure 4. Adhesion maps obtained using QI™ mode for (a) 296 K (b) 308 K and (c) 323 K. (d) Normalized adhesion taken for three different samples as a function of temperature.

For further proof of the formation of dry phospholipid bilayers, we draw on a more detailed study of well-known behaviour of conventionally wet produced SLBs. Attwood et al. [38] and Gosvami [39] described an AFM-tip induced change in morphology of SLBs on mica produced by vesicles in water (DOPC, DPPC) and by the Langmuir–Blodgett (LB) technique (DODAB), respectively. In both cited studies, AFM measurements performed in water show a morphological modification of the scan area due to the interaction of the SLB with the cantilever tip. We analysed the tip-surface interaction as a function of temperature and compared our AFM measurements with temperature-dependent ellipsometric analysis. The latter is a non-invasive method, based on low energy photon-solid interaction, which does not affect the structure of the molecules nor the morphology of the crystalline or fluid ordered phases. In other words, we analysed the topographical channels as a function of temperature to study structural changes in the film. Figure 5 shows AFM topography images before and after temperature ramps, i.e., from room temperature (RT) to 347 K, performed within the ellipsometer (Figure 5a–c) and within the AFM (Figure 5d–f). Figure 5a shows the topography of the evaporated SLBs at RT before the first temperature ramp was performed within the ellipsometer. In Figure 5b,c, we observe the sample at RT after the first and sixth temperature ramp carried out within the ellipsometer, respectively. A reorganization of the initial surface (Figure 5a) into an even more homogeneous bilayer surface is observed (Figure 5b,c). In order to study the reorganization of the sample shown in Figure 5a–c, we perform temperature cycles within AFM to map the surface topography with increasing temperature operating in air. AFM topography images were taken every 5 K, starting from RT up to 343 K. Figure 5d shows the topography of the evaporated DPPC sample before any temperature ramp. The morphology of Figure 5d is similar to that of Figure 5a. Figure 5e shows the AFM topography of the SLBs after the first temperature ramp was performed within the AFM in the same scanning zone as Figure 5d. Figure 5f shows the AFM topography of the same sample after the first temperature in a contiguous region to the scanned area shown in Figure 5e, i.e., it was not imaged during the temperature cycle. The scanned area during the temperature cycle (Figure 5e) has a roughness parameter of $R_q = 28$ nm, while the contiguous region (Figure 5f) has a roughness of $R_q = 3.3$ nm.

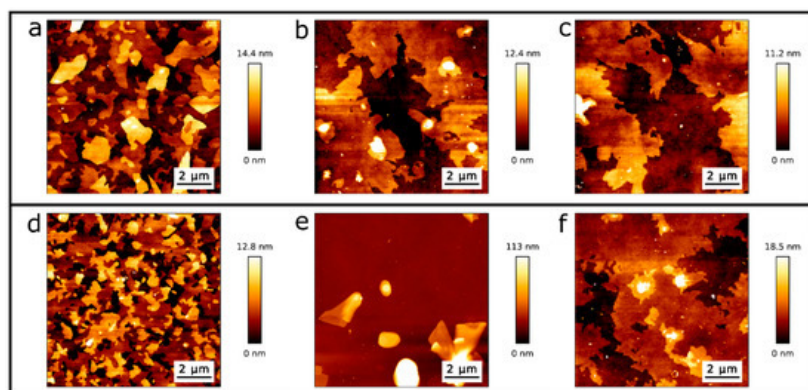


Figure 5. Topographic AFM images from DPPC/SiO₂/Si samples at RT: (a) directly after evaporation and before the first temperature cycle, (b) after the first and (c) sixth temperature cycle performed within the ellipsometer. (d) Topography image directly after evaporation and before temperature cycling within the AFM, (e) after the first temperature cycle while scanning with AFM, and (f) after the first temperature cycle in a contiguous region to the scanned area.

To quantify the effect of the tip-SLB interaction, we perform AFM imaging in air at RT of the DPPC single- and double bilayers. In Figure 6, we observe the area reduction of a double bilayer and a single bilayer induced by the AFM tip. A total of 10 AFM images were recorded. The first five images were taken at a force setpoint of 1 nN (Figure 6a–c), while the following five were taken at 3 nN (Figure 6d–f), which is below the measured breakthrough force in Figure 2. From the topographical images of Figure 6, we observed a clear reduction in the double bilayer area, as well as a restructuring of the single bilayer.

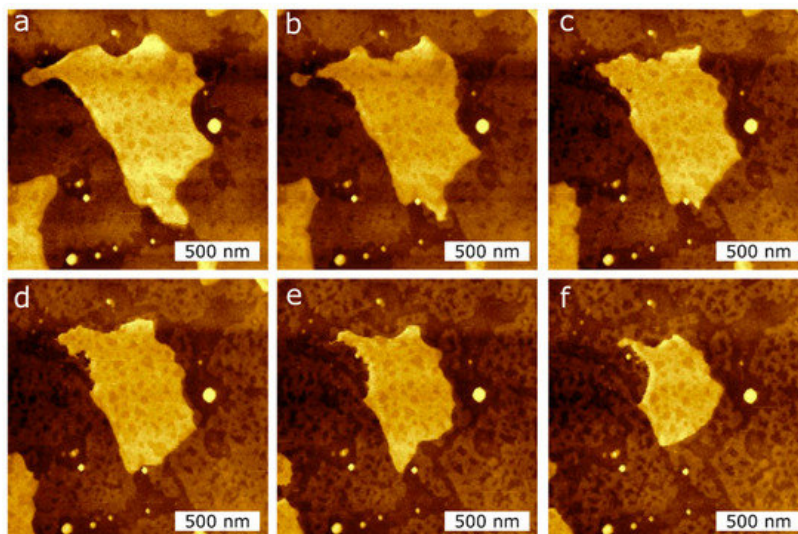


Figure 6. AFM topography images of the DPPC bilayer taken at RT in air during consecutive measurements in the same scan region ($2\ \mu\text{m} \times 2\ \mu\text{m}$) to induce the reduction of the island-like DPPC bilayer surface area, applying two different tip forces, (a–c): 1 nN; (d–f): 3 nN.

We measured the area of the DPPC islands seen in Figure 6 by masking the image by height using an image processor (Gwyddion) and obtain the area as a function of scan number, for two different applied tip forces. Figure 7 shows the reduction in area of the DPPC islands as a function of scan number. For scan numbers 1–5, the applied force was 1 nN, and for scan numbers 6–10, 3 nN. The measured area reduction follows a linear behaviour and there is a clear difference in rates between two applied tip forces. For a set point of 1 nN the measured reduction rate was $-2.4 \times 10^4\ \text{nm}^2/\text{scan}$ and for 3 nN we obtain $-6.5 \times 10^4\ \text{nm}^2/\text{scan}$.

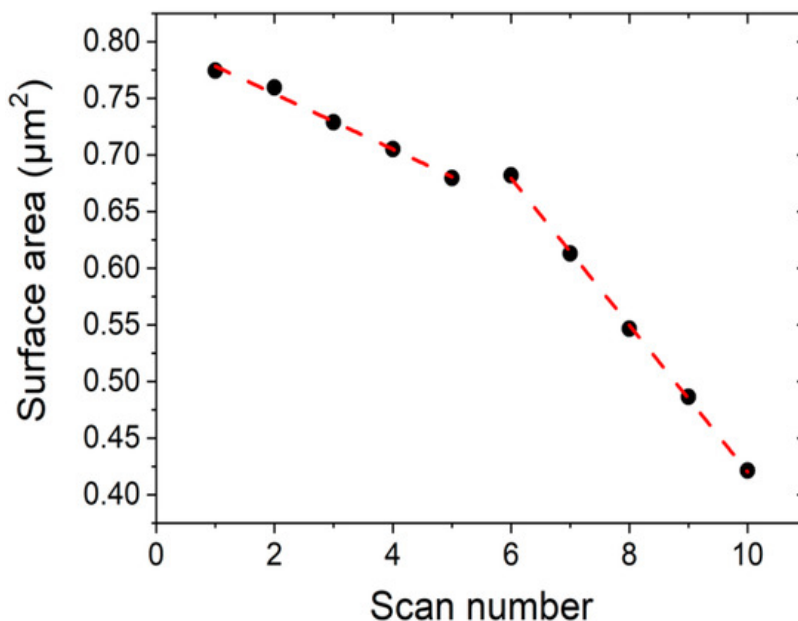


Figure 7. Surface area reduction during consecutive scans at RT using two different tip forces applied in the same scan regions. Scans 1–5 are taken at 1 nN, while scans 6–10 are taken at 3 nN.

Author also analysed the depth of the holes created by the AFM tip in the SLBs, as seen in the second bilayer island of Figure 6. The average hole depth is $1.2 \pm 0.4\ \text{nm}$, as measured by cross-sections over the hole. These holes are lower in height than a DPPC monolayer thickness, and do not change with the different setpoints used, i.e., 1 nN and 3 nN.

References

1. van Doremalen, N.; Bushmaker, T.; Morris, D.; Holbrook, M.; Gamble, A.; Williamson, B.; Tamin, A.; Harcourt, J.; Thornburg, N.; Gerber, S.; et al. Aerosol and surface stability of HCoV-19 (SARS-CoV-2) compared to SARS-CoV-1. *Engl. J. Med.* 2020, 382, 1564–1567 doi:10.1056/NEJMc2004973
2. Kustanovich, K.; Yantchev, V.; Doosti, B.A.; Gözen, I.; Jesorka, A. A microfluidics-integrated impedance/surface acoustic resonance tandem sensor. *Bio-Sensing Res.* 2019, 25, 100291, doi:https://doi.org/10.1016/j.sbsr.2019.100291.
3. Czolkos, I.; Jesorka, A.; Orwar, O. Molecular phospholipid films on solid supports. *Soft Matter* 2011, 7, 4562–4576, doi:10.1039/c0sm01212b.
4. Alessandrini, A.; Facci, P. Phase transitions in supported lipid bilayers studied by AFM. *Soft Matter* 2014, 10, 7145–7164, doi:10.1039/c4sm01104j.
5. Rother, M.; Nussbaumer, M.G.; Renggli, K.; Bruns, N. Protein cages and synthetic polymers: A fruitful symbiosis for drug delivery applications, bionanotechnology and materials science. *Soc. Rev.* 2016, 45, 6213–6249, doi:10.1039/c6cs00177g.
6. Ni, M.; Zhuo, S. Applications of self-assembling ultrashort peptides in bionanotechnology. *RSC Adv.* 2019, 9, 844–852, doi:10.1039/C8RA07533F.
7. Sun, Q.; Du, Y.; Zhao, Z.; Hall, E.A.H.; Gao, H.; Sukhorukov, G.B.; Routh, A.F. Functional Silver-Coated Colloidosomes as Targeted Carriers for Small Molecules. *Langmuir* 2017, 33, 3755–3764, doi:10.1021/acs.langmuir.6b04594.
8. Bhaskar, S.; Lim, S. Engineering protein nanocages as carriers for biomedical applications. *NPG Asia Mater.* 2017, 9, e371, doi:10.1038/am.2016.128.
9. Shalev, O.; Raghavan, S.; Mazzara, J.M.; Senabulya, N.; Sinko, P.D.; Fleck, E.; Rockwell, C.; Simopoulos, N.; Jones, C.M.; Schwendeman, A.; et al. Printing of small molecular medicines from the vapor phase. *Commun.* 2017, 8, 1–9, doi:10.1038/s41467-017-00763-6.
10. Albert, K.; Huang, X.C.; Hsu, H.Y. Bio-templated silica composites for next-generation biomedical applications. *Colloid Interface Sci.* 2017, 249, 272–289, doi:10.1016/j.cis.2017.04.011.
11. Richter, R.P.; Bérat, R.; Brisson, A.R. Formation of solid-supported lipid bilayers: An integrated view. *Langmuir* 2006, 22, 3497–3505, doi:10.1021/la052687c.
12. Gözen, I.; Dommersnes, P.; Czolkos, I.; Jesorka, A.; Lobovkina, T.; Orwar, O. Fractal avalanche ruptures in biological membranes. *Mater.* 2010, 9, 908–912, doi:10.1038/nmat2854.
13. Castellana, E.T.; Cremer, P.S. Solid supported lipid bilayers: From biophysical studies to sensor design. *Sci. Rep.* 2006, 61, 429–444, doi:10.1016/j.surfrep.2006.06.001.
14. Pace, H.; Simonsson Nyström, L.; Gunnarsson, A.; Eck, E.; Monson, C.; Geschwindner, S.; Snijder, A.; Höök, F. Preserved Transmembrane Protein Mobility in Polymer-Supported Lipid Bilayers Derived from Cell Membranes. *Chem.* 2015, 87, 9194–9203, doi:10.1021/acs.analchem.5b01449.
15. Mazur, F.; Bally, M.; Städler, B.; Chandrawati, R. Liposomes and lipid bilayers in biosensors. *Colloid Interface Sci.* 2017, 249, 88–99, doi:10.1016/j.cis.2017.05.020.
16. Tero, R.; Takizawa, M.; Li, Y.J.; Yamazaki, M.; Urisu, T. Lipid membrane formation by vesicle fusion on silicon dioxide surfaces modified with alkyl self-assembled monolayer islands. *Langmuir* 2004, 20, 7526–7531, doi:10.1021/la0400306.
17. Plant, A.L.; Brigham-Burke, M.; Petrella, E.; O'Shannessy, D. Phospholipid/Alkanethiol Bilayers for Cell-Surface Receptor Studies by Surface Plasmon Resonance. *Biochem.* 1995, 226, 342–348.
18. Lingler, S.; Rubinstein, I.; Knoll, W.; Offenhäusser, A. Fusion of small unilamellar lipid vesicles to alkanethiol and thiolipid self-assembled monolayers on gold. *Langmuir* 1997, 13, 7085–7091, doi:10.1021/la970600k.
19. Andersson, J.; Köper, I. Tethered and polymer supported bilayer lipid membranes: Structure and function. *Membranes* 2016, 6, 30, doi:10.3390/membranes6020030.
20. Rebaud, S.; Maniti, O.; Girard-Egrot, A.P. Tethered bilayer lipid membranes (tBLMs): Interest and applications for biological membrane investigations. *Biochimie* 2014, 107, 135–142, doi:10.1016/j.biochi.2014.06.021.
21. Sumitomo, K.; Oshima, A. Liquid-Ordered/Liquid-Crystalline Phase Separation at a Lipid Bilayer Suspended over Microwells. *Langmuir* 2017, 33, 13277–13283, doi:10.1021/acs.langmuir.7b02156.
22. Zhu, Z.W.; Wang, Y.; Zhang, X.; Sun, C.F.; Li, M.G.; Yan, J.W.; Mao, B.W. Electrochemical impedance spectroscopy and atomic force microscopic studies of electrical and mechanical properties of nano-black lipid membranes and size

dependence. *Langmuir* 2012, 28, 14739–14746, doi:10.1021/la303047v.

23. Kurniawan, J.; Ventrici De Souza, J.F.; Dang, A.T.; Liu, G.Y.; Kuhl, T.L. Preparation and Characterization of Solid-Supported Lipid Bilayers Formed by Langmuir-Blodgett Deposition: A Tutorial. *Langmuir* 2018, 34, 15622–15639, doi:10.1021/acs.langmuir.8b03504.
24. Maekawa, T.; Chin, H.; Nyu, T.; Sut, T.N.; Ferhan, A.R.; Hayashi, T.; Cho, N.-J. Molecular diffusion and nano-mechanical properties of multi-phase supported lipid bilayers. *Chem. Chem. Phys.* 2019, 21, 16686–16693, doi:10.1039/c9cp02085c.
25. Retamal, M.J.; Cisternas, M.A.; Gutierrez-Maldonado, S.E.; Perez-Acle, T.; Seifert, B.; Busch, M.; Huber, P.; Volkmann, U.G. Towards bio-silicon interfaces: Formation of an ultra-thin self-hydrated artificial membrane composed of dipalmitoylphosphatidylcholine (DPPC) and chitosan deposited in high vacuum from the gas-phase. *Chem. Phys.* 2014, 141, 104201–104207, doi:10.1063/1.4894224.
26. Leonenko, Z. V.; Finot, E.; Ma, H.; Dahms, T.E.S.; Cramb, D.T. Investigation of temperature-induced phase transitions in DOPC and DPPC phospholipid bilayers using temperature-controlled scanning force microscopy. *J.* 2004, 86, 3783–3793, doi:10.1529/biophysj.103.036681.
27. Duncan, S.L.; Dalal, I.S.; Larson, R.G. Molecular dynamics simulation of phase transitions in model lung surfactant monolayers. *Biophys. Acta* 2011, 1808, 2450–2465, doi:10.1016/j.bbamem.2011.06.026.
28. Mabrey, S.; Sturtevant, J.M. Investigation of phase transitions of lipids and lipid mixtures by high sensitivity differential scanning calorimetry. *Natl. Acad. Sci. USA* 1976, 73, 3862–3866.
29. Petri, W.A.; Estep, T.N.; Pal, R.; Thompson, T.E.; Biltonen, R.L.; Wagner, R.R. Thermotropic behavior of dipalmitoylphosphatidylcholine vesicles reconstituted with the glycoprotein of vesicular stomatitis virus. *Biochemistry* 1980, 19, 3088–3091.
30. Wiacek, A.E.; Holysz, L.; Chibowski, E. Effect of temperature on n-tetradecane emulsion in the presence of phospholipid DPPC and enzyme lipase or phospholipase A2. *Langmuir* 2008, 24, 7413–7420, doi:10.1021/la800794x.
31. Retamal, M.J.; Corrales, T.P.; Cisternas, M.A.; Moraga, N.H.; Diaz, D.I.; Catalan, R.E.; Seifert, B.; Huber, P.; Volkmann, U.G. Surface Morphology of Vapor-Deposited Chitosan: Evidence of Solid-State Dewetting during the Formation of Biopolymer Films. *Biomacromolecules* 2016, 17, 1142–1149, doi:10.1021/acs.biomac.5b01750.
32. Cisternas, M.; Bhuyan, H.; Retamal, M.J.; Casanova-Morales, N.; Favre, M.; Volkmann, U.G.; Saikia, P.; Diaz-Droguett, D.E.; Mändl, S.; Manova, D.; et al. Study of nitrogen implantation in Ti surface using plasma immersion ion implantation & deposition technique as biocompatible substrate for artificial membranes. *Mater. Sci. Eng. C.* 2020, 113, 111002, doi:https://doi.org/10.1016/j.msec.2020.111002.
33. Balgavý, P.; Dubničková, M.; Kučerka, N.; Kiselev, M.A.; Yaradaikin, S.P.; Uhríková, D. Bilayer thickness and lipid interface area in unilamellar extruded 1,2-diacylphosphatidylcholine liposomes: A small-angle neutron scattering study. *Biochim. Biophys. Acta—Biomembr.* 2001, 1512, 40–52.
34. Alessandrini, A.; Seeger, H.M.; Di Cerbo, A.; Caramaschi, T.; Facci, P. What do we really measure in AFM punch-through experiments on supported lipid bilayers? *Soft Matter* 2011, 7, 7054–7064.
35. Dignam, M.J.; Fedyk, J. Infrared Ellipsometric Spectroscopy of Adsorbed Species. *Appl. Spectrosc. Rev.* 1978, 14, 249–285.
36. Drude, P. Zur Elektronentheorie der Metalle. *Ann. Phys.* 1900, 306, 556.
37. Cisternas, E.A.; Corrales, T.P.; del Campo, V.; Soza, P.A.; Volkmann, U.G.; Bai, M.; Taub, H.; Hansen, F.Y. Crystalline-to-plastic phase transitions in molecularly thin n-dotriacontane films adsorbed on solid surfaces. *J. Chem. Phys.* 2009, 131, 114705.
38. Attwood, S.J.; Choi, Y.; Leonenko, Z. Preparation of DOPC and DPPC supported planar lipid bilayers for atomic force microscopy and atomic force spectroscopy. *Int. J. Mol. Sci.* 2013, 14, 3514–3539.
39. Gosvami, N.N.; Parsons, E.; Marcovich, C.; Berkowitz, M.L.; Hoogenboom, B.W.; Perkin, S. Resolving the structure of a model hydrophobic surface: DODAB monolayers on mica. *RSC Adv.* 2012, 2, 4181–4188.